Recommendation ITU-R P.531-15

(08/2023)

P Series: Radiowave propagation

Ionospheric propagation data and prediction methods required for the design of satellite networks and systems

Foreword

The role of the Radiocommunication Sector is to ensure the rational, equitable, efficient and economical use of the radio-frequency spectrum by all radiocommunication services, including satellite services, and carry out studies without limit of frequency range on the basis of which Recommendations are adopted.

The regulatory and policy functions of the Radiocommunication Sector are performed by World and Regional Radiocommunication Conferences and Radiocommunication Assemblies supported by Study Groups.

Policy on Intellectual Property Right (IPR)

ITU-R policy on IPR is described in the Common Patent Policy for ITU-T/ITU-R/ISO/IEC referenced in Resolution ITU-R 1. Forms to be used for the submission of patent statements and licensing declarations by patent holders are available from http://www.itu.int/ITU-R/go/patents/en where the Guidelines for Implementation of the Common Patent Policy for ITU-T/ITU-R/ISO/IEC and the ITU-R patent information database can also be found.

Series of ITU-R Recommendations

(Also available online at https://www.itu.int/publ/R-REC/en)

Series	Title
BO	Satellite delivery
BR	Recording for production, archival and play-out; film for television
BS	Broadcasting service (sound)
BT	Broadcasting service (television)
F	Fixed service
M	Mobile, radiodetermination, amateur and related satellite services
P	**Radiowave propagation**
RA	Radio astronomy
RS	Remote sensing systems
S	Fixed-satellite service
SA	Space applications and meteorology
SF	Frequency sharing and coordination between fixed-satellite and fixed service systems
SM	Spectrum management
SNG	Satellite news gathering
TF	Time signals and frequency standards emissions
V	Vocabulary and related subjects

Note: *This ITU-R Recommendation was approved in English under the procedure detailed in Resolution ITU-R 1.*

Electronic Publication
Geneva, 2023

© ITU 2023

RECOMMENDATION ITU-R P.531-15

Ionospheric propagation data and prediction methods required for the design of satellite networks and systems

(Question ITU-R 218/3)

(1978-1990-1992-1994-1997-1999-2001-2003-2005-2007-2009-2012-2013-2016-2019-2023)

Scope

Recommendation ITU-R P.531 describes a method for evaluating the ionospheric propagation effects on paths between Earth and space (at frequencies from 0.1 to 12 GHz) "OR" (at frequencies above the ionosphere critical frequency, where the ionosphere becomes transparent to radiowaves, to several tens of gigahertz). The following effects may take place on paths between Earth and space when the signal is passing through the ionosphere:

–   rotation of the polarization (Faraday rotation) due to the interaction of the electromagnetic wave with the ionized medium in the Earth's magnetic field along the path;

–   group delay and phase advance of the signal due to the total electron content (TEC) accumulated along the path;

–   rapid variation of amplitude and phase (scintillations) of the signal due to small-scale irregular structures in the ionosphere;

–   a change in the apparent direction of arrival due to refraction;

–   Doppler effects due to non-linear polarization rotations and time delays.

The data and methods described in this Recommendation are applicable for planning satellite systems, in respective ranges of validity indicated in Annex 1.

Keywords

Trans-ionospheric propagation, scintillation, group delay

Abbreviations/Glossary

MUF: Maximum usable frequency

TEC: Total electron content

XPD: Cross-polarisation discrimination

Related ITU Recommendations, Reports

Recommendation ITU-R P.618

Recommendation ITU-R P.844

Recommendation ITU-R P.1239

Report ITU-R P.2097

Report ITU-R P.2297

NOTE – In every case the latest edition of the Recommendation/Reports in force should be used.

The ITU Radiocommunication Assembly,

considering

a)   that the ionosphere causes significant propagation effects at frequencies up to at least 12 GHz;

b)   that effects may be particularly significant for non-geostationary-satellite orbit services below 3 GHz;

c)   that experimental data have been presented and/or modelling methods have been developed that allow the prediction of the ionospheric propagation parameters needed in planning satellite systems;

d)   that ionospheric effects may influence the design and performance of radio systems involving spacecraft;

e)   that these data and methods have been found to be applicable, within the natural variability of propagation phenomena, for applications in any satellite network/system planning,

recommends

that the data prepared and methods developed as set out in Annex 1 should be used for planning satellite systems, in the respective ranges of validity indicated in Annex 1.

Annex 1

1   Introduction

This Annex deals with the ionospheric propagation effects on paths between Earth and space.

Dependent upon the application, the ionospheric effects may be negligible at frequencies higher than about 12 GHz. The lower frequency of applicability of the information given here will be somewhat higher than the ordinary wave critical frequency, for which monthly median and decile estimates are given in Recommendation ITU-R P.1239, depending on the path geometry. Trans-ionospheric propagation at LF and lower frequencies has been discussed in CCIR Report 262-7 (1990) and is not addressed here.

From a system design viewpoint, the impact of ionospheric effects can be summarized as follows:

a)   the total electron content (TEC) accumulated along a satellite service transmission path penetrating the ionosphere causes rotation of the wave polarization (Faraday rotation), time delay of the signal, and a change in the apparent direction of arrival due to refraction;

b)   localized random ionospheric patches, commonly referred to as ionospheric irregularities, further cause excess and random rotations and time delays, which can only be described in stochastic terms;

c)   because the rotations and time delays relating to electron density are non-linearly frequency dependent, both a) and b) further result in dispersion or group velocity distortion;

d)   furthermore, localized ionospheric irregularities also act like convergent and divergent lens which focus and defocus the radio waves. Such effects are commonly referred to as the scintillations which affect amplitude, phase and angle-of-arrival of the signal.

Due to the complex nature of ionospheric physics, system parameters affected by ionospheric effects as noted above cannot always be succinctly summarized in simple analytic formulae. Relevant data edited in terms of tables and/or graphs, supplemented with further descriptive or qualifying statements, are for all practical purposes the best way to present the effects.

In considering propagation effects between the Earth and space at frequencies below 3 GHz, one has to recognize that:

e)   the normally known propagation effects between the Earth and space caused by hydrometeors are not significant relative to effects of f);

f)   the near surface multipath effects, in the presence of natural or man-made obstacles at low elevation angles, are always critical;

g)   the near surface multipath effects vary from locality to locality, and therefore they do not dominate the overall propagation between the Earth and space when global scale propagation factors are to be dealt with.

2   Background

Caused by solar radiation, the Earth's ionosphere consists of several regions of ionization. For all practical communications purposes, regions of the ionosphere, D, E, F and top-side ionization have been identified as contributing to the TEC between satellite and ground terminals.

In each region, the ionized medium is neither homogeneous in space nor stationary in time. Generally speaking, the background ionization has relatively regular diurnal, seasonal and 11-year solar cycle variations, and is dependent strongly on geographical locations and geomagnetic activity. In addition to the background ionization, there are always highly dynamic, small-scale non-stationary structures known as irregularities. Both the background ionization and irregularities degrade radiowaves. Furthermore, the refractive index is frequency dependent, i.e. the medium is dispersive.

3   Considerations for VHF and HF propagation

For VHF signals propagated within and through the ionosphere, as the operating frequency decreases distortion and degradation of the signal becomes increasingly severe until the ionosphere cannot be penetrated and transmissions from space stations are refracted upwards or transmissions from earth stations are refracted back to the ground. Since the ionosphere is very variable in structure and density, the frequency at which this will occur is also variable and will also depend on the path geometry.

For a space station where the antenna illuminates paths which would become geometrically tangential to the ionosphere at heights of about 200-300 km, this penetration frequency would be given approximately by the MUF(4000)F2 given by $(1.1 \times M(3000) \ F2 \times foF2)$. Monthly median and decile estimates of M(3000)F2 and foF2 are given in Recommendation ITU-R P.1239. The 1% values for the 4 000 km MUF is also given in maps in Recommendation ITU-R P.844. It is not clear to what the 1% refers, but it is possibly for all hours in the months of the solar maximum year of 1958. That was the most extreme solar maximum that has ever been observed. However such geometrical considerations may be too simplistic. Propagation within the ionosphere at angles close to tangential may be within a duct giving propagation to longer ranges and being subject to effects due to ionospheric irregularities.

At the other extreme, for antennas directed at the nadir, the penetration frequency will be the maximum plasma frequency, foF2.

It is concluded that, for the ionospheric effects listed in Table 3, the frequency dependences will apply to frequencies as low as 100 MHz, except possibly at times and locations with very severe ionospheric disturbances. At lower frequencies down to the maximum plasma frequency (foF2) for vertical incidence propagation, earth-space propagation will still be expected but the practicality of a radiocommunication service will depend on the specific system design, application and required reliability.

4   Prime degradations due to background ionizations

A number of effects, such as refraction, dispersion and group delay, are in magnitude directly proportional to the TEC; Faraday rotation is also approximately proportional to TEC, with the contributions from different parts of the ray path weighted by the longitudinal component of magnetic field. A knowledge of the TEC thus enables many important ionospheric effects to be estimated quantitatively.

4.1   TEC

Denoted as N_T, the TEC can be evaluated by:

$$N_T = \int_s n_e(s)\, ds \tag{1}$$

where:

$\quad\quad\quad s:$ propagation path (m)

$\quad\quad\quad n_e:$ electron concentration (el/m^3).

Even when the precise propagation path is known, the evaluation of N_T is difficult because n_e has diurnal, seasonal and solar cycle variations.

For modelling purposes, the TEC value is usually quoted for a zenith path having a cross-section of 1 m^2. The TEC of this vertical column can vary between 10^{16} and 10^{18} el/m^2 with the peak occurring during the sunlit portion of the day.

For estimating the TEC, a procedure based on § 4.1.1 is described below. This is also suitable for slant path TEC.

4.1.1   NeQuick2-based method

The electron density distribution given by the model is represented by a continuous function that is also continuous in all spatial first derivatives. It consists of two parts, the bottom-side part (below the peak of the F2-layer) and the top-side part (above the F2-layer peak). The peak height of the F2-layer is calculated from M(3000)F2 and the ratio foF2/foE (see Recommendation ITU-R P.1239).

The bottom-side is described by semi-Epstein layers for representing E, F1 and F2. The top-side F layer is again a semi-Epstein layer with a height dependent thickness parameter. The NeQuick2 v.P531-12 model gives the electron density and TEC along arbitrary ground-to-satellite or satellite-to-satellite paths.

The computer program and associated data files are integral digital products to this Recommendation and are available in the file Rec P 531-15 Part 1 Supplement ZIP.zip from the supplement file <u>R-REC-P.531-15-202308-I!!ZIP-E.zip</u>.

4.2   Faraday rotation

When propagating through the ionosphere, a linearly polarized wave will suffer a gradual rotation of its plane of polarization due to the presence of the geomagnetic field and the anisotropy of the plasma medium. The magnitude of Faraday rotation, θ, will depend on the frequency of the radiowave, the magnetic field strength, and the electron density of the plasma as:

$$\theta = 2.36 \times 10^{-14} \frac{B_{av} N_T}{f^2} \tag{2}$$

where:
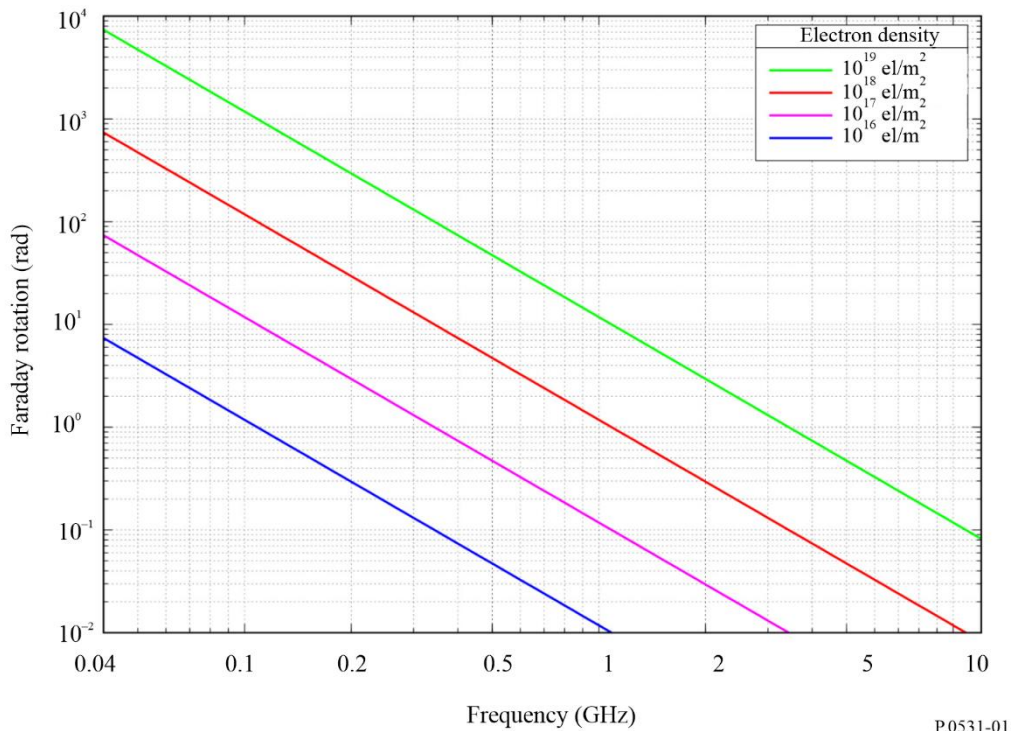
θ : angle of rotation (rad)

B_{av} : average Earth magnetic field (Wb $\cdot$ m^{-2} or T)

f : frequency (GHz)

N_T : TEC (el $\cdot$ m^{-2}).

Example values of θ for B_{av} , the average value of the Earth's magnetic field strength, of 50 µT are shown in Fig. 1.

FIGURE 1

Faraday rotation as a function of TEC and frequency

The Faraday rotation is thus inversely proportional to the square of frequency and directly proportional to the integrated product of the electron density and the component of the Earth's magnetic field along the propagation path. Its median value at a given frequency exhibits a very regular diurnal, seasonal, and solar cyclical behaviour that can be predicted. This regular component of the Faraday rotation can therefore be compensated for by a manual adjustment of the polarization tilt angle at the earth station antennas. However, large deviations from this regular behaviour can occur for small percentages of the time as a result of geomagnetic storms and, to a lesser extent, large-scale travelling ionospheric disturbances. These deviations cannot be predicted in advance. Intense and fast fluctuations of the Faraday rotation angles of VHF signals have been associated with strong and fast amplitude scintillations respectively, at locations situated near the crests of the equatorial anomaly.

The cross-polarization discrimination for aligned antennas, XPD (dB), is related to the Faraday rotation angle, θ, by:

$$XPD = -20 \log (\tan \theta) \qquad (3)$$

4.3   Group delay

The presence of charged particles in the ionosphere slows down the propagation of radio signals along the path. The time delay in excess of the propagation time in free space, commonly denoted as t, is called the group delay. It is an important factor to be considered for any satellite network/systems. Likewise, the phase is advanced by the same amount. This quantity can be computed as follows:

$$t = 1.345\, N_T/f^2 \times 10^{-7} \qquad\qquad (4)$$

where:

t: delay time (s) with reference to propagation in a vacuum

f: frequency of propagation (Hz)

N_T: determined along the slant propagation path (el/m^2).

Figure 2 is a plot of time delay, t, versus frequency, f, for several values of electron content along the ray path.

For a band of frequencies around 1 600 MHz the signal group delay varies from approximately 0.5 to 500 ns, for TEC from 10^{16} to 10^{19} el/m^2. Figure 3 shows the yearly percentage of daytime hours that the time delay will exceed 20 ns at a period of relatively high solar activity.

Equation (4) gives the phase advance but with opposite sign.

4.4   Dispersion

When trans-ionospheric signals occupy a significant bandwidth the propagation delay (being a function of frequency) introduces dispersion. The differential delay across the bandwidth is proportional to the integrated electron density along the ray path. For a fixed bandwidth the relative dispersion is inversely proportional to frequency cubed. Thus, systems involving wideband transmissions must take this effect into account at VHF and possibly UHF. For example, as shown in Fig. 4 for an integrated electron content of 5×10^{17} el/m^2, a signal with a pulse length of 1 μs will sustain a differential delay of 0.02 μs at 200 MHz while at 600 MHz the delay would be only 0.00074 μs (see Fig. 4).

4.5   TEC rate of change

With an orbiting satellite the observed rate of change of TEC is due in part to the change of direction of the ray path and in part to a change in the ionosphere itself. For a satellite at a height of 22 000 km traversing the auroral zone, a maximum rate of change of 0.7×10^{16} el/m^2/s has been observed. For navigation purposes, such a rate of change corresponds to an apparent velocity of 0.11 m/s.

FIGURE 2

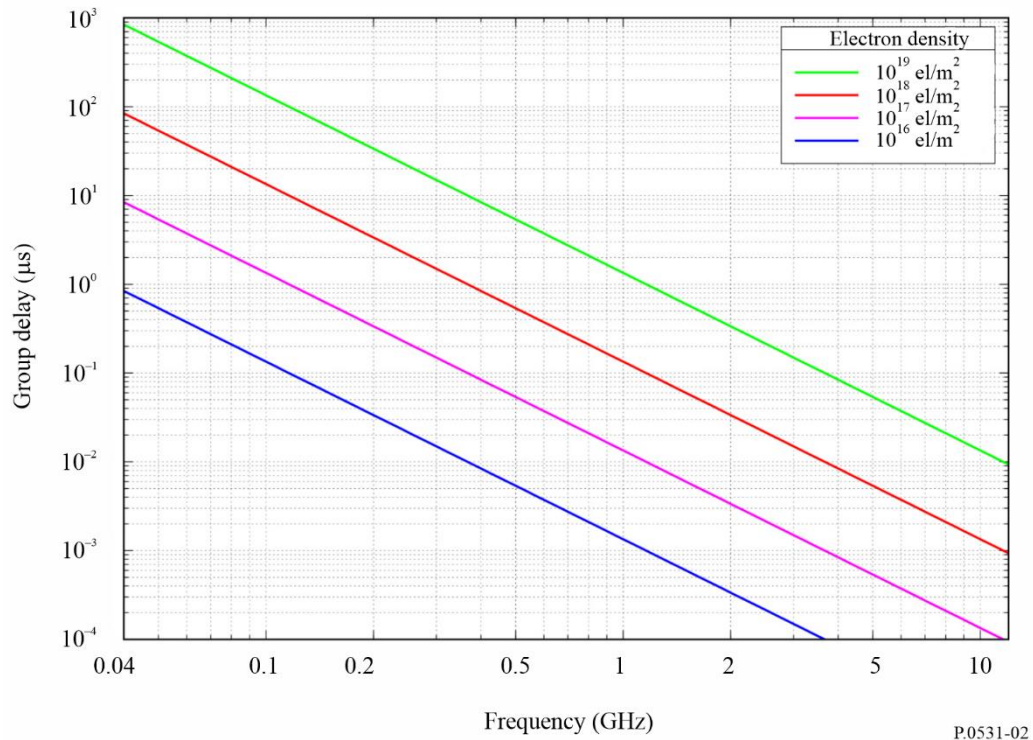**Ionospheric time delay versus frequency for various values of electron content**

P.0531-02

FIGURE 3

Contours of percentage of yearly average daytime hours when time delay at vertical incidence at 1.6 GHz exceeds 20 ns (sunspot number = 140)
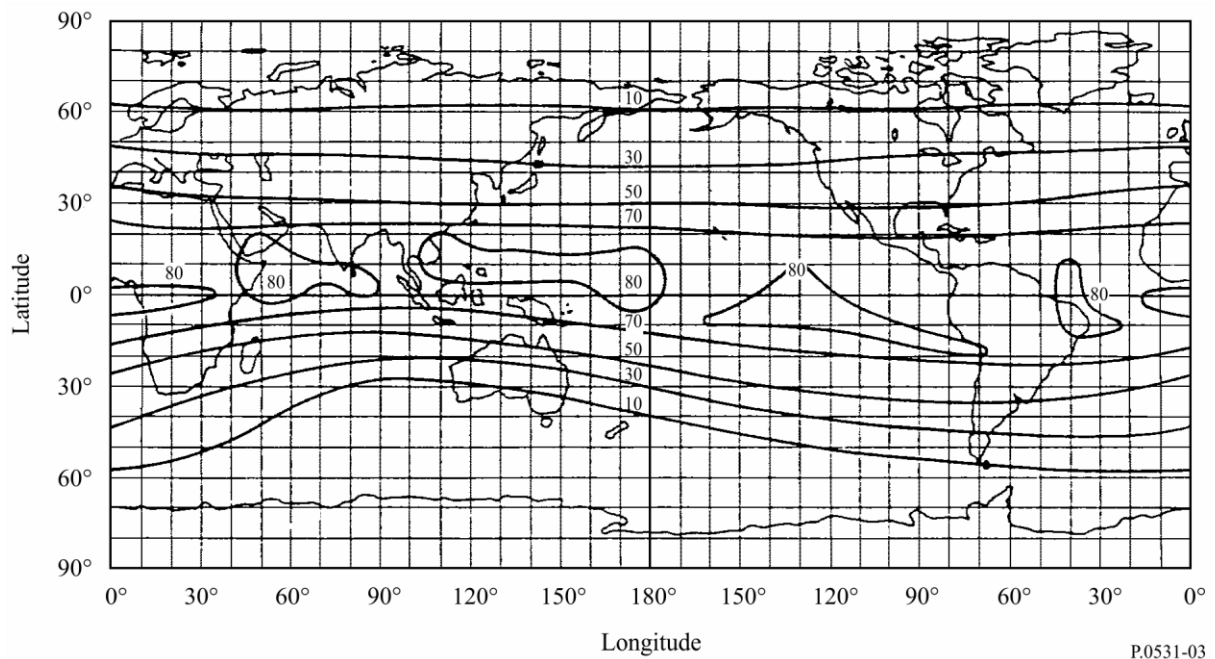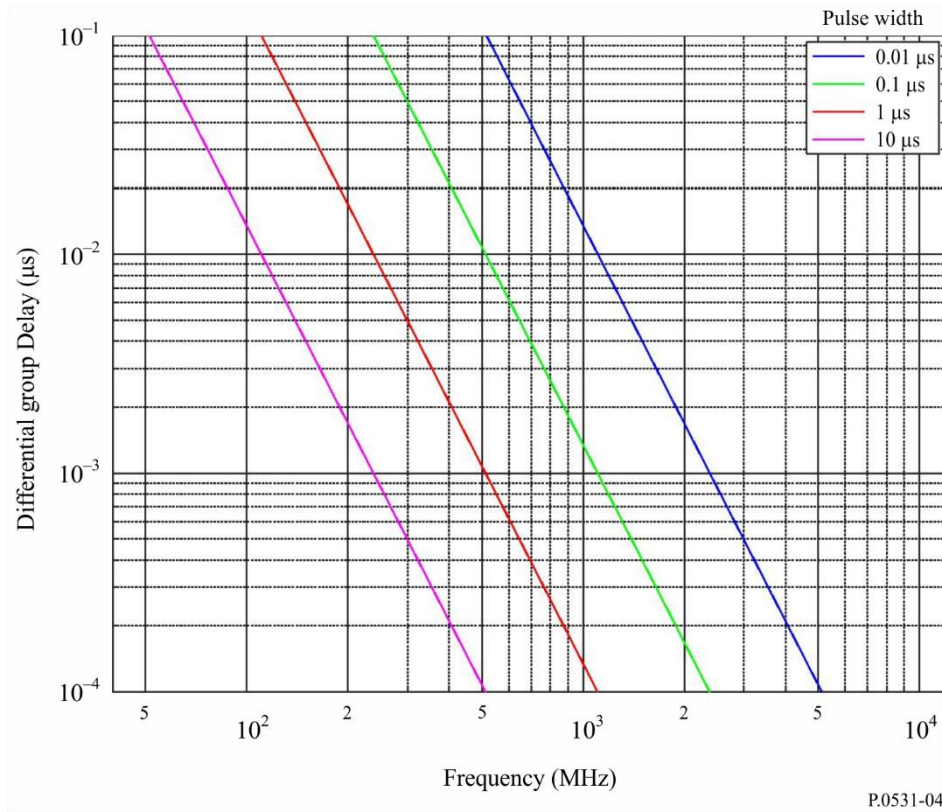

P.0531-03

FIGURE 4

**Difference in the time delay between the lower and upper frequencies of the spectrum
of a pulse of width, τ, transmitted through the ionosphere,
one way traversal, with TEC equal to 5×10^{17} el/m^2**

P.0531-04

5   Principal degradation due to irregularities

5.1   Scintillation

One of the most severe disruptions along a trans-ionospheric propagation path for signals below 3 GHz is caused by ionospheric scintillation. Ionospheric scintillation effects may be observed occasionally up to 10 GHz. Scintillations are created by fluctuations of the refractive index, which are caused by inhomogeneities in the medium. At the receiver, the signal exhibits rapid amplitude and phase fluctuations, and modifications to its time coherence properties. Principally through the mechanisms of forward scattering and diffraction, small-scale irregular structures in the ionization density cause scintillation phenomena in which the steady signal at the receiver is replaced by one which is fluctuating in amplitude, phase and apparent direction of arrival. Depending on the modulation of the system, various aspects of scintillation affect the system performance differently. The most commonly used parameter characterizing the intensity fluctuations is the scintillation index S_4, defined by equation (5):

$$S_4 = \left(\frac{\langle I^2 \rangle - \langle I \rangle^2}{\langle I \rangle^2} \right)^{1/2} \tag{5}$$

where I is the intensity of the signal (proportional to the square of the signal amplitude) and $\langle \; \rangle$ denotes averaging.

The scintillation index S_4 is related to the peak-to-peak fluctuations of the intensity. The exact relationship between the scintillation index S_4 and the peak-to-peak fluctuations of the intensity
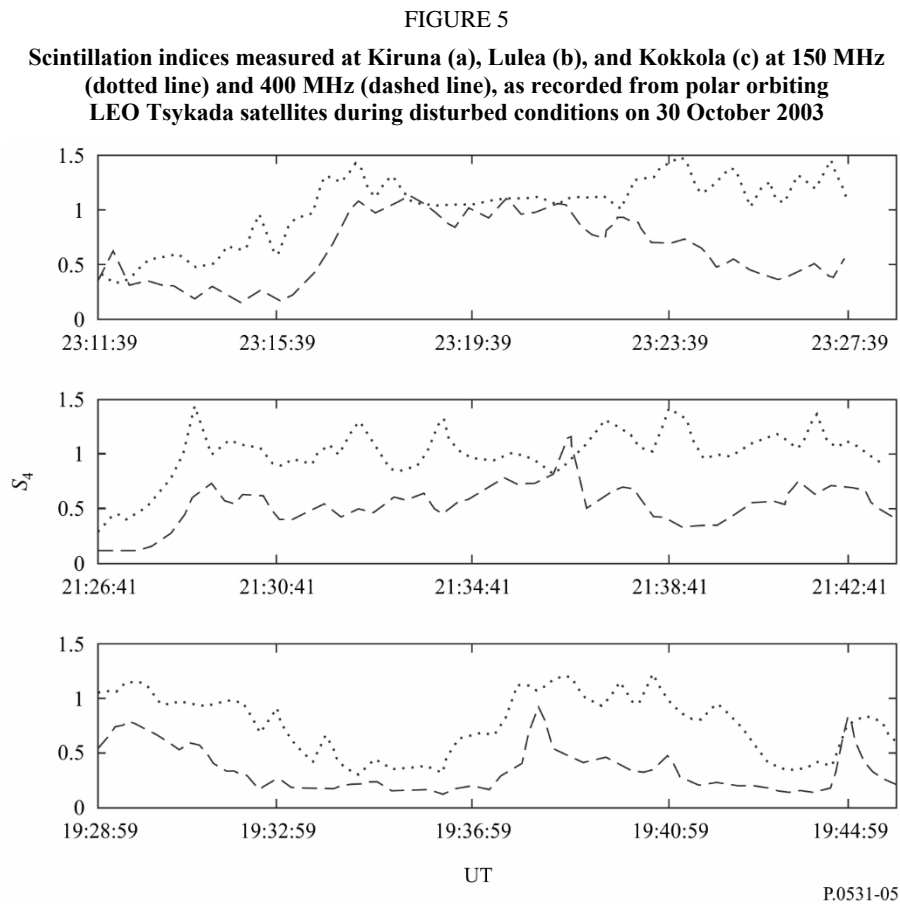
depends on the distribution of the intensity and the detrending algorithm for the intensity related to the computation procedure of the scintillation index S_4. The intensity distribution is best described by the Nakagami distribution for a wide range of S_4 values.

Scintillation strength may, for convenience, be classified into three regimes: weak, moderate or strong. The weak values correspond to $S_4 < 0.3$, the moderate values from 0.3 to 0.6 and the strong case for $S_4 > 0.6$.

For weak and moderate regimes, S_4 shows a consistent $f^{-\upsilon}$ frequency dependence, with υ being 1.5 for most multifrequency observations. In addition for weak regimes the amplitude follows a log-normal distribution.

In the strong regime, it has been observed that the υ factor decreases. This is due to the saturation of scintillation under the strong influence of multiple scattering. As S_4 approaches 1.0, the intensity follows a Rayleigh distribution. Occasionally, S_4 may exceed 1, reaching values as high as 1.5. Figure 5 shows an example of the frequency dependence of S_4 at VHF and UHF for three auroral stations for weak, moderate and strong scintillations.

The phase scintillations follow a Gaussian distribution with zero mean. The standard deviation is used to characterize the phase scintillations (σ_φ). For weak and moderate regimes, most observations in equatorial regions indicate that phase and intensity scintillation are strongly correlated; S_4 and σ_φ (when expressed in radians) have similar values.

FIGURE 5

Scintillation indices measured at Kiruna (a), Lulea (b), and Kokkola (c) at 150 MHz (dotted line) and 400 MHz (dashed line), as recorded from polar orbiting LEO Tsykada satellites during disturbed conditions on 30 October 2003

P.0531-05

Empirically, Table 1 provides a convenient conversion between S_4 and the approximate peak-to-peak fluctuations P_{fluc} (dB), when the S_4 index is not greater than 1.0. This relationship can be approximated by:

$$P_{fluc} = 27.5 \, S_4^{1.26} \tag{6}$$

where $0.0 \le S_4 \le 1.0$.

TABLE 1

Empirical conversion table for scintillation indices

S_4	P_{fluc} (dB)
0.1	1.5
0.2	3.5
0.3	6
0.4	8.5
0.5	11
0.6	14
0.7	17
0.8	20
0.9	24
1.0	27.5

Future studies could change the validity and range of equation (6).

5.2   Geographic, seasonal and solar dependence of scintillations

Geographically, there are two intense zones of scintillation, one at high latitudes and the other centred within ± 20° of the magnetic equator as shown in Fig. 6. Severe scintillation has been observed up to gigahertz frequencies in these two sectors, while in the middle latitudes scintillation occurs exceptionally, such as during geomagnetic storms. In the equatorial sector, there is a pronounced night-time maximum of activity as also indicated in Figs 6 and 7. For equatorial gigahertz scintillation, peak activity around the vernal equinox and high activity at the autumnal equinox have been observed.

A typical scintillation event has its on-set after local ionospheric sunset and an event can last from 30 min to hours. For equatorial stations in years of solar maximum, ionospheric scintillation occurs almost every evening after sunset, with the peak-to-peak fluctuations of signal level at 4 GHz exceeding 10 dB in magnitude.

5.3   Ionospheric scintillation model

In order to predict the intensity of ionospheric scintillation paths between the Earth and space, it is recommended that the Global Ionospheric Scintillation Model (GISM) be used. The GISM permits one to predict the S_4 index, the depth of amplitude fading as well as the rms phase and angular deviations due to scintillation as a function of satellite and ground station locations, date, time and working frequency. The model is based on the multiple phase screen method. The main internal parameters of the model are set to the following default values:

−   Slope of the intensity spectrum, $p = 3$

−   Average size of the irregularities, $L_0 = 500$ km

−   Standard deviation of the electron density fluctuations, $\sigma_{Ne} = 0.2$.

The bending of the rays is taken into account and the characteristics of the background ionosphere are computed in a sub-routine which uses the NeQuick2 ionospheric model. The source code and program of the GISM is an integral digital product to this Recommendation and is available in the file Rec P.531-14 Part 2 Supplement ZIP.zip from the supplement file R-REC-P.531-15-202308-I!!ZIP-E.zip.

5.4 Instantaneous statistics and spectrum behaviour

5.4.1 Instantaneous statistics

During an ionospheric scintillation event, the Nakagami density function is believed to be adequately close for describing the statistics of the instantaneous variation of amplitude. The density function for the intensity of the signal is given by:

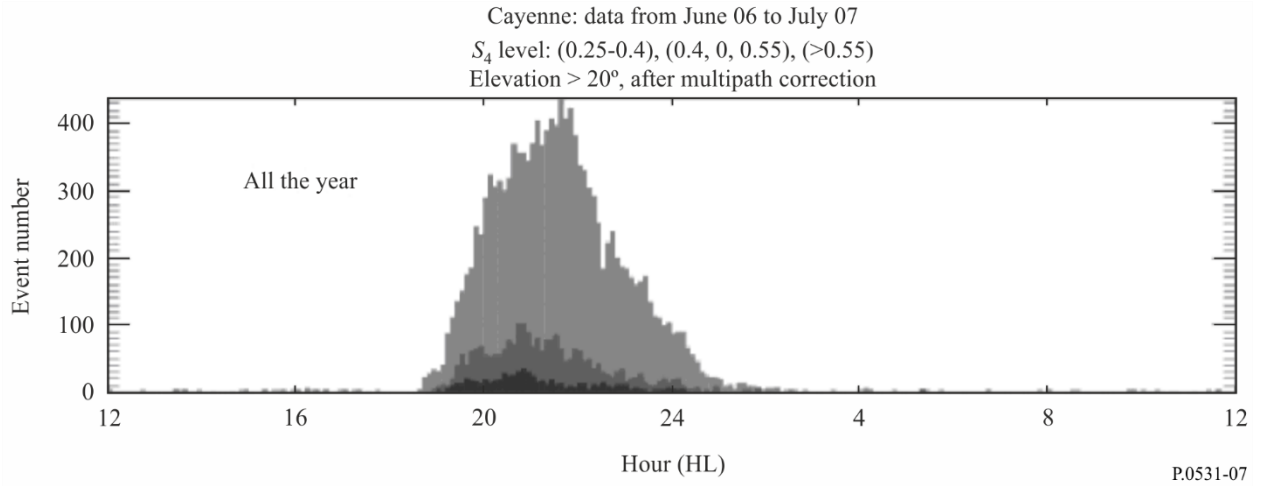$$p(I) = \frac{m^m}{\Gamma(m)} I^{m-1} \exp(-mI) \tag{7}$$

FIGURE 6

Depth of scintillation fading (proportional to density of cross-hatching) at 1.5 GHz during solar maximum and minimum years
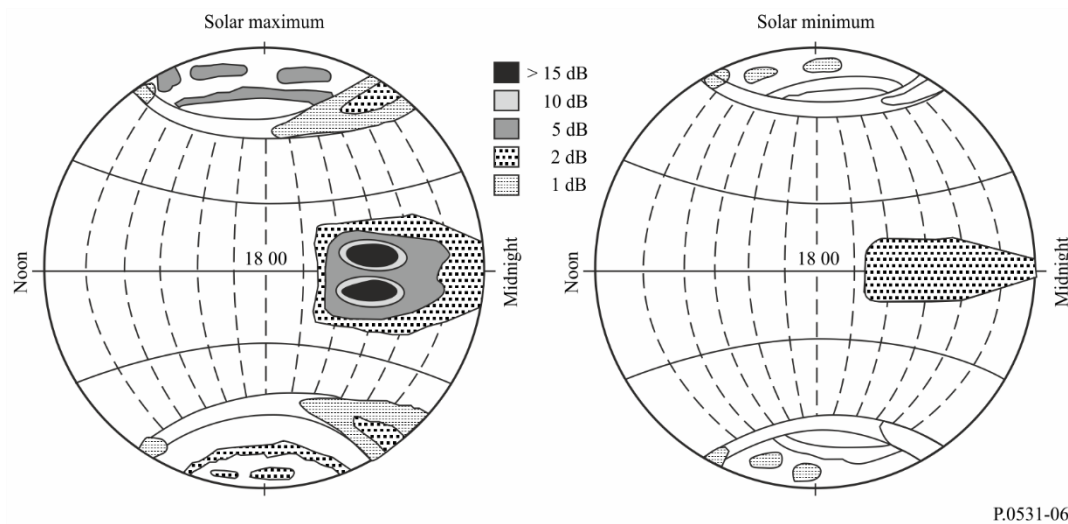
P.0531-06

FIGURE 7

Distribution of one year scintillation events at Cayenne during June 06 to July 07;
S_4 level weak (top); moderate (middle); strong (bottom) for elevation angles > 20°

Cayenne: data from June 06 to July 07
S_4 level: (0.25-0.4), (0.4, 0, 0.55), (>0.55)
Elevation > 20°, after multipath correction

P.0531-07

where the Nakagami "m-coefficient" is related to the scintillation index, S_4 by:

$$m = \exp\left(5.69 * \exp(-3.055 * S_4) + 0.292 * \exp(0.344 * S_4)\right) \tag{8}$$

where $0.1 \leq S_4 \leq 1.0$.

In formulating equation (7) the average intensity level of I is normalized to be 1.0. The calculation of the fraction of time that the signal is above or below a given threshold is greatly facilitated by the fact that the distribution function corresponding to the Nakagami density has a closed form expression which is given by:

$$P(I) = \int\limits_0^I p(x)\,dx = \frac{\Gamma(m, mI)}{\Gamma(m)} \tag{9}$$

where $\Gamma(m, mI)$ and $\Gamma(m)$ are the incomplete gamma function and gamma function, respectively. Using equation (9), it is possible to compute the fraction of time that the signal is above or below a given threshold during an ionospheric event. For example, the fraction of time that the signal is more than X dB below the mean is given by $P(10^{-X/10})$ and the fraction of time that the signal is more than Y dB above the mean is given by $1 - P(10^{Y/10})$.

5.4.2   Spectrum behaviour

In terms of temporal characteristics, the fading rate of ionospheric scintillation is about 0.1 to 1 Hz. The spatial and temporal power spectra exhibit a wide range of slopes, from f^{-1} to f^{-6} as have been reported from different observations. A typical spectrum behaviour is shown in Fig. 8. The f^{-3} slope as shown is recommended for system applications if direct measurement results are not available. This value is representative of weak to moderate scintillation events.

The roll-off frequency differs from amplitude and phase scintillation as shown in Fig. 9. Phase scintillation presents more pronounced low frequency components than amplitude scintillation.

5.5 Geometric consideration

5.5.1 Zenith angle dependence

In most models, S_4^2 is shown to be proportional to the secant of the zenith angle, i, of the propagation path. This relationship is believed to be valid up to $i \approx 70°$ for weak and moderate scintillation levels. At greater zenith angles, a dependence ranging between 1/2 and first power of sec i should be used.

5.5.2 Seasonal-longitudinal dependence

The occurrence of scintillations and magnitude of S_4 have a longitudinal as well as seasonal dependence that can be parameterized by the angle, β, shown in Fig. 11. It is the angle between the sunset terminator and local magnetic meridian at the apex of the field line passing through the line-of-sight at the height of the irregularity slab. The weighting function for seasonal-longitudinal dependence is given by:

$$S_4 \propto \exp[-(\frac{\beta}{W})^2] \tag{10}$$

where W is a weighting constant depending on location as well as calendar day of the year. As an example, using the data available from Tangua, Hong Kong and Kwajalein, the numerical value of the weighting constant can be modelled as shown in Fig. 12.

FIGURE 8

Power spectral density estimates for a geostationary satellite (Intelsat-IV) at 4 GHz
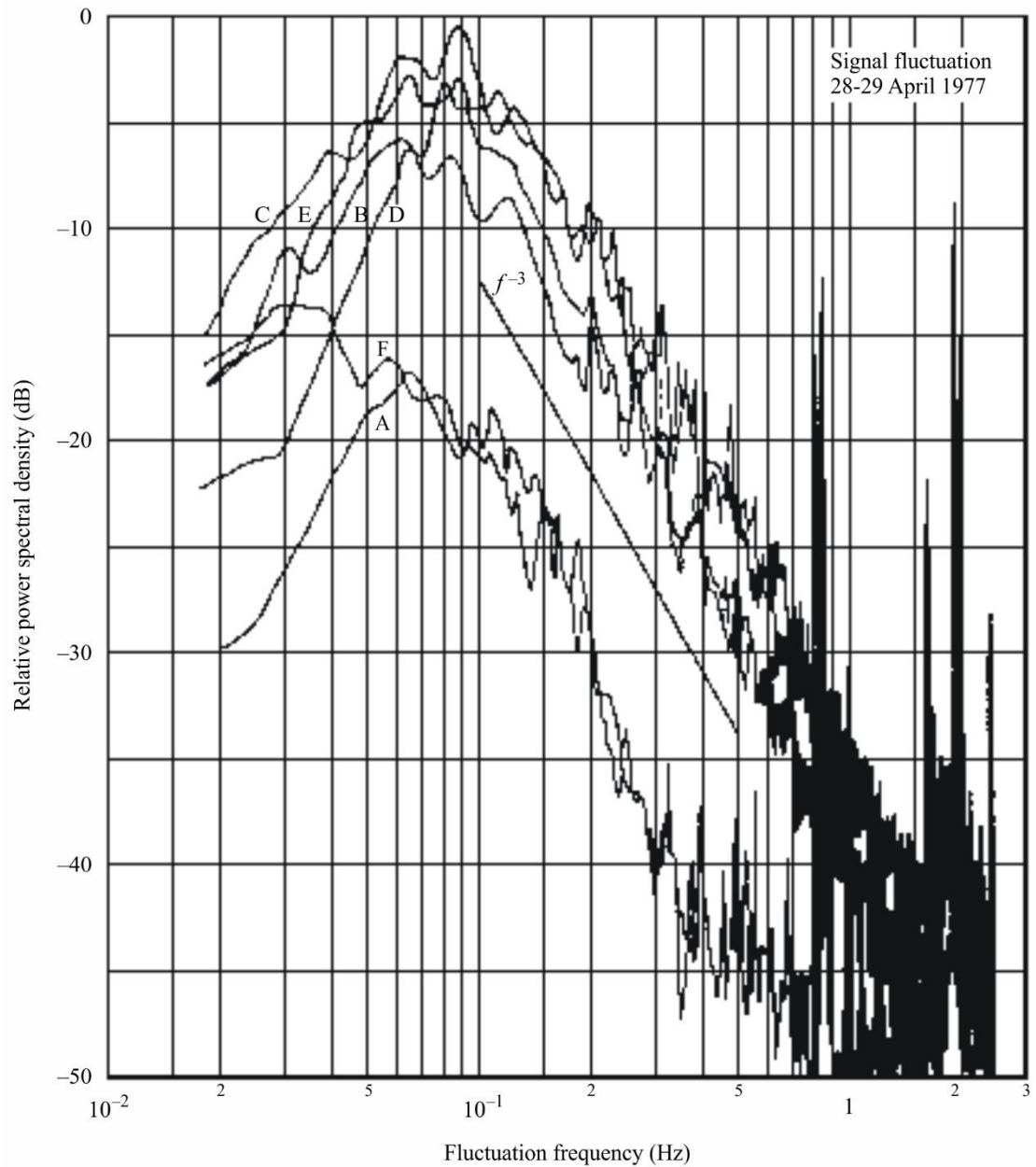
The scintillation event was observed during the evenings
of 28-29 April 1977 at Taipei earth station

A: 30 min before event onset
B: at the beginning
C: 1 h after
D: 2 h after
E: 3 h after
F: 4 h after

P.0531-08

FIGURE 9
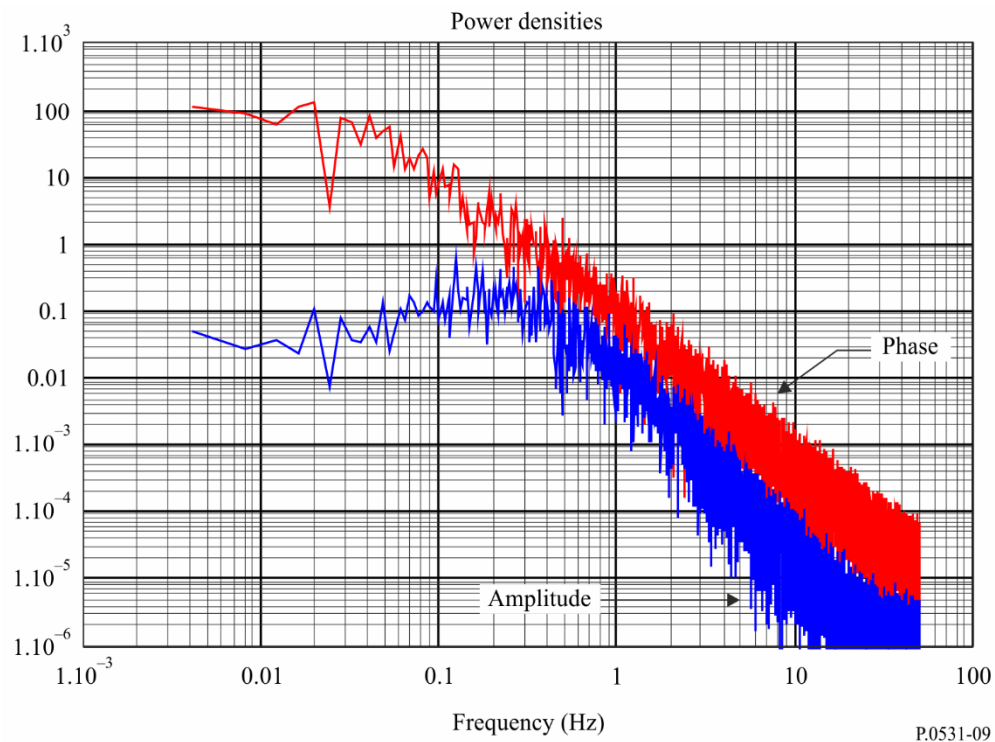
Typical intensity and phase spectrum

P.0531-09

FIGURE 10

Intersection of the propagation path with a magnetic field line at the F-region height

P.0531-10
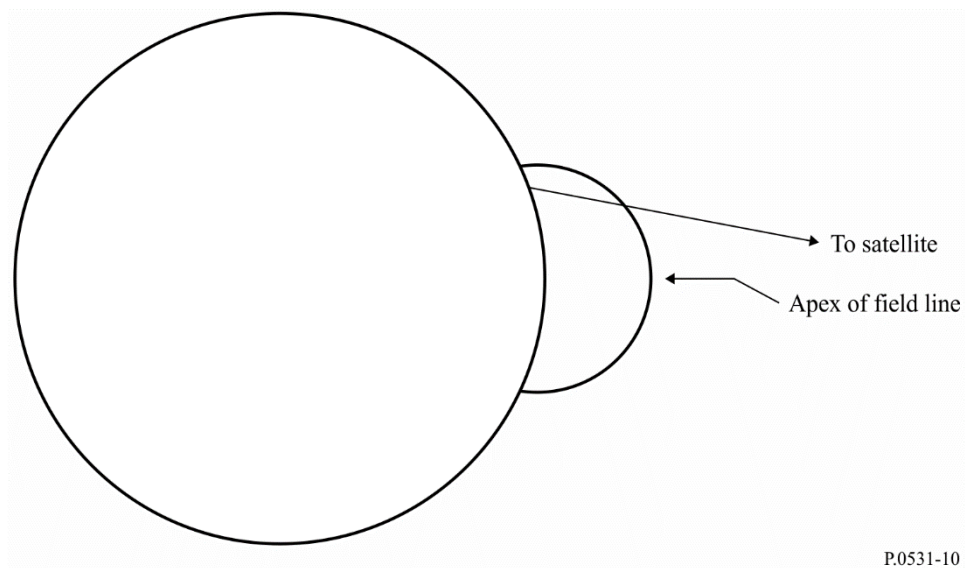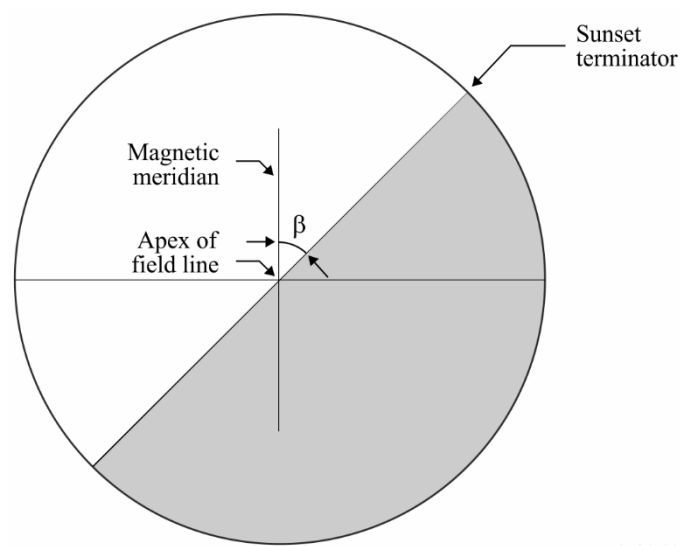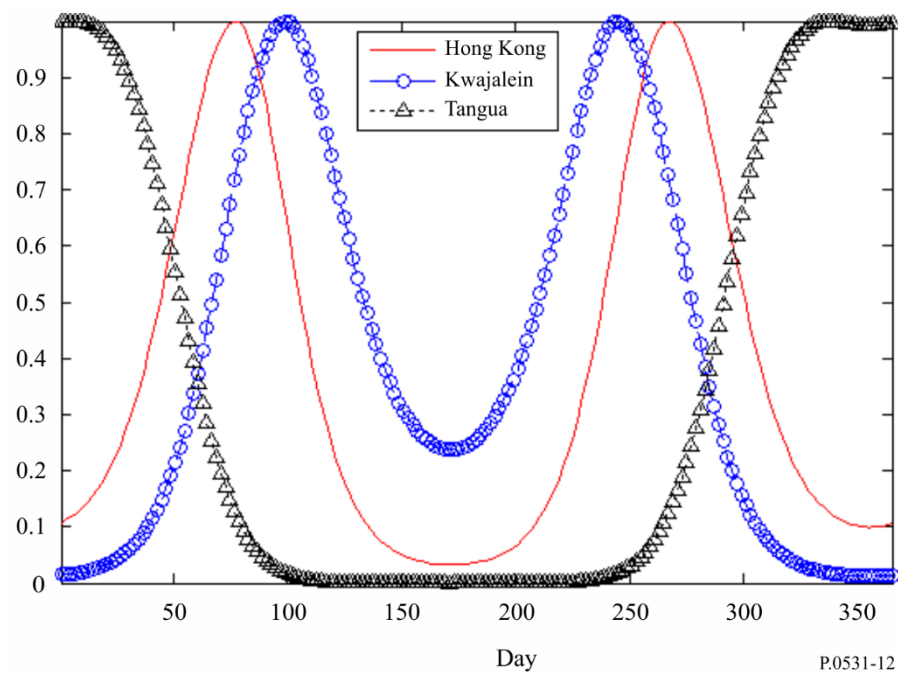
FIGURE 11

**Angle between the local magnetic meridian at the apex of the field line
shown in Fig. 10 and the sunset terminator**

P.0531-11

FIGURE 12

Seasonal weighting functions for stations in different longitude sectors

P.0531-12

5.6 Cumulative statistics

When considering the design of satellite radiocommunication systems and the assessment of frequency sharing, communications engineers have concerns not only with the system degradation and interference during an event but also with the long-term cumulative occurrence statistics. For communications systems involving a geostationary satellite, which is the simplest radio system configuration, Figs 13 and 14 are recommended for the assessment and scaling of occurrence statistics. The sunspot numbers cited are the 12 month averaged sunspot numbers.

The long-term cumulative distribution, $P(I)$, of the signal intensity relative to its mean value can be derived from the long-term cumulative statistics, $F(\xi)$, of the peak-to-peak fluctuation, ξ, such as those found in Fig. 14, as follows:

$$P(I) = \sum_{i=0}^{n} f_i \, P_i(I) \tag{11}$$

where:

$$f_0 = F\,(\xi < \xi_1) \tag{11a}$$

$$f_i = F\,(\xi_i \le \xi < \xi_{i+1}) \qquad (i = 1, 2, \ldots, n-1) \tag{11b}$$

$$f_n = F\,(\xi \ge \xi_n) \tag{11c}$$

and ξ_1 and ξ_n are the minimum and maximum peak-to-peak fluctuation values, respectively, and n is the interval number of ξ of interest to the user:

$$P_i(I) = \Gamma\,(m_i, m_i I) \,/\, \Gamma(m_i) \tag{11d}$$

$$m_i = \exp\left(5.69 * \exp(-3.055 * S_{4i}) + 0.292 * \exp(0.344 * S_{4i})\right) \tag{11e}$$

$$S_{40} = \left[\frac{1}{27.5} \cdot \frac{\xi_1}{2}\right]^{1/1.26} \tag{11f}$$

$$S_{4i} = \left[\frac{1}{27.5} \cdot \frac{\xi_i + \xi_{i+1}}{2}\right]^{1/1.26} \qquad (i = 1, 2, \ldots n-1) \tag{11g}$$

$$S_{4n} = \left[\frac{1}{27.5} \cdot \frac{\xi_{n-1} + 3\,\xi_n}{4}\right]^{1/1.26} \tag{11h}$$

Figure 15 shows an example of long-term cumulative distribution of signal intensity derived from the curve P6 of Fig. 14.

5.7 Simultaneous occurrence of ionospheric scintillation and rain fading

Ionospheric scintillation and rain fading are two impairments of completely different physical origin. However, in equatorial regions at years of high sunspot number, the simultaneous occurrence of the two effects may have an annual percentage time that is significant to system design. The cumulative simultaneous occurrence time was about 0.06% annually as noted at 4 GHz at Djutiluhar earth station in Indonesia.

The simultaneous events have signatures that are often vastly different from those when only a single impairment, either scintillation or rain alone, is present. While ionospheric scintillation alone is not a depolarization phenomenon, and rain fading alone is not a signal fluctuation phenomenon (although it may cause slight fluctuations of polarization for moderate to strong scintillations), the simultaneous events produce a significant amount of signal fluctuations in the cross-polarization channel.

Recognition of these simultaneous events is needed for applications on any satellite network/system which requires high availability.

The prediction of rain fading is described in Recommendation ITU-R P.618.

FIGURE 13

**Dependence of 4 GHz equatorial ionospheric scintillations
on monthly mean sunspot number**
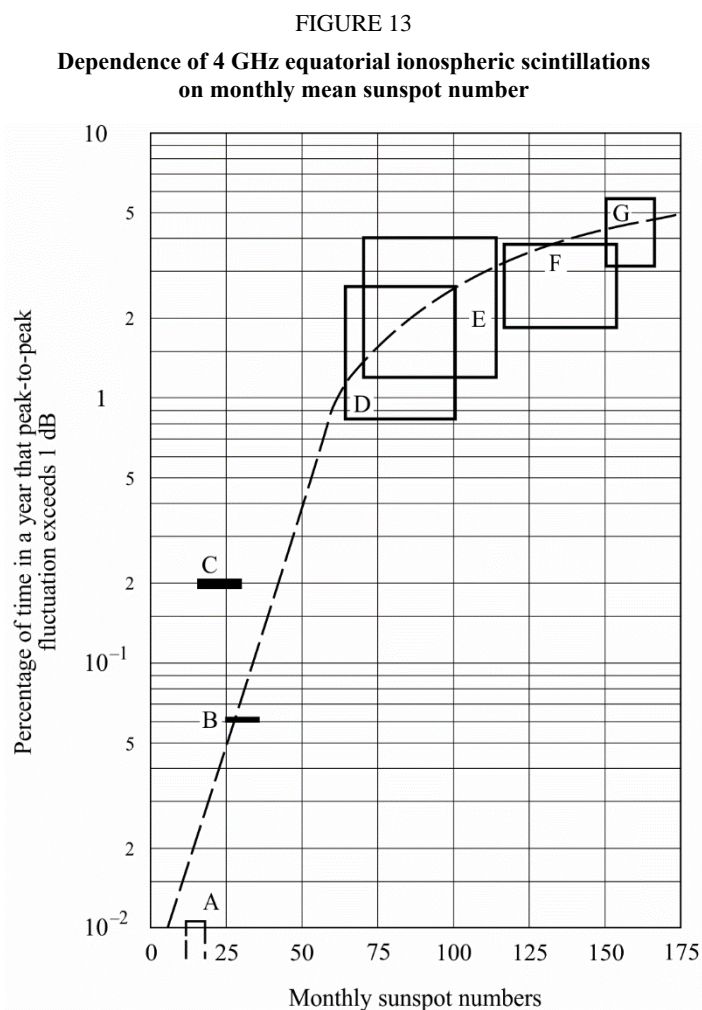
The squares are the ranges of variations over a year
for different carriers

A: 1975-1976, Hong Kong and Bahrein, 15 carriers
B: 1974, Longovilo, 1 carrier
C: 1976-1977, Taipei, 2 carriers
D: 1970-1971, 12 stations, > 50 carriers
E: 1977-1978, Hong Kong, 12 carriers
F: 1978-1979, Hong Kong, 10 carriers
G: 1979-1980, Hong Kong, 6 carriers

P.0531-13

5.8   Gigahertz scintillation model

To evaluate the scintillation effects that can be expected in a given situation the following steps may be used:

Step 1: Figure 14 provides scintillation occurrence statistics on equatorial ionospheric paths: peak-to-peak amplitude fluctuations, P_{fluc}, (dB), for 4 GHz reception from satellites in the East at elevation angles of about 20° (P solid curves) and in the West at about 30° elevation (I dotted curves). The data are given for different times of year and sunspot number.

Step 2: Since Fig. 14 relates to 4 GHz, values for other frequencies are found by multiplying these values by $(f/4)^{-1.5}$ where f is the frequency of interest (GHz).

Step 3: The variation of P_{fluc} with geographical location and diurnal occurrence can be qualitatively estimated from Fig. 6.

Step 4: As one element of link budget calculations, P_{fluc} is related to signal loss L_p by $L_p = P_{fluc}/\sqrt{2}$.

Step 5: The scintillation index S_4, the most widely used parameter in describing scintillation, is defined in § 5.1 and may be obtained from P_{fluc} using Table 1.

FIGURE 14

**Annual statistics of peak-to-peak fluctuations observed at Hong Kong earth station
(Curves I1, P1, I3-I6, P3-P6) and Taipei earth station (Curves P2 and I2)**
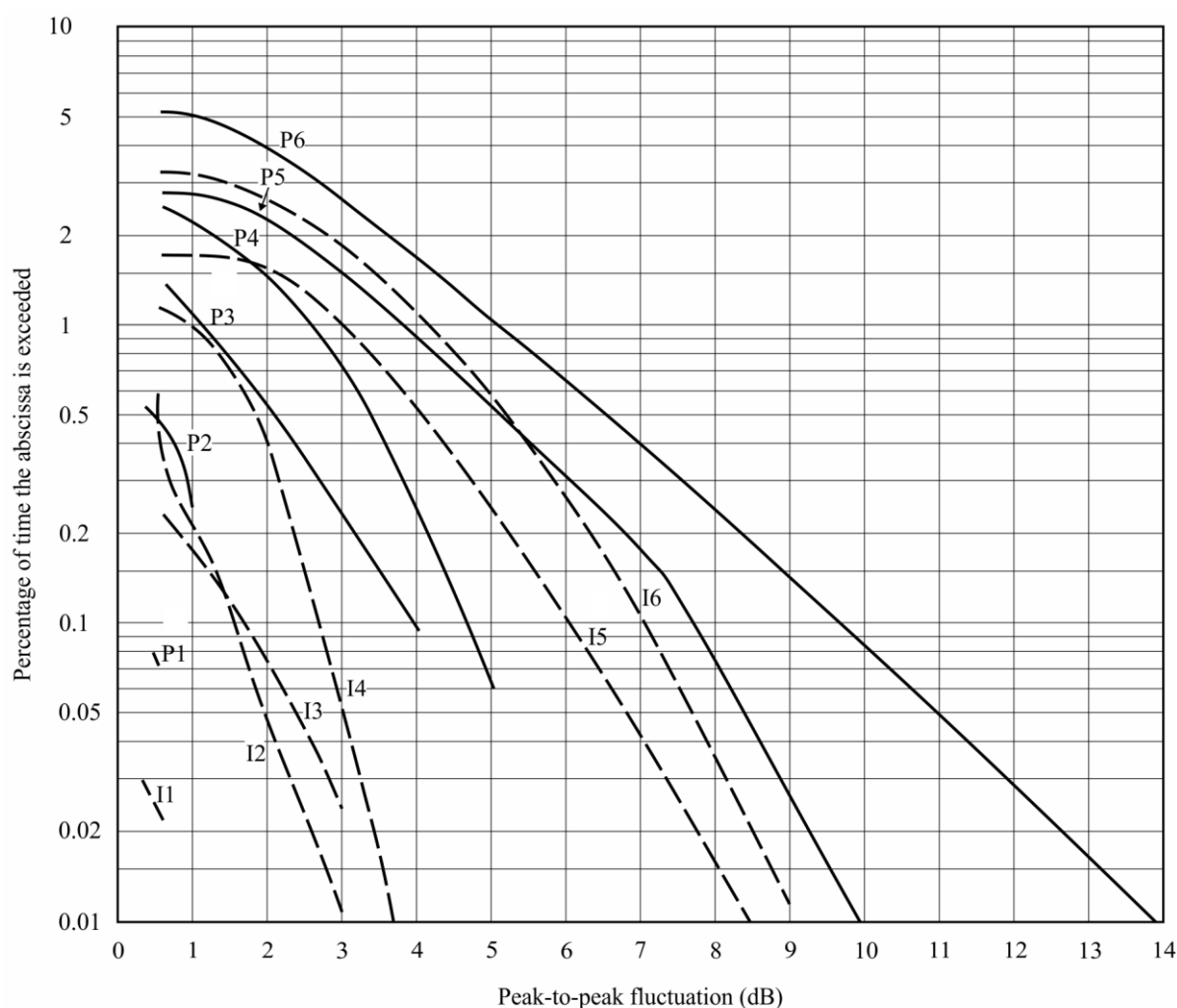
Curve	Period	SSN range
I1, P1	March 75-76	10-15
I2, P2	June 76-77	12-26
I3, P3	March 77-78	20-70
I4, P4	October 77-78	44-110
I5, P5	November 78-79	110-160
I6, P6	June 79-80	153-165

P.0531-14

FIGURE 15

An example of long-term cumulative statistics of signal intensity (4 GHz, 20° elevation)
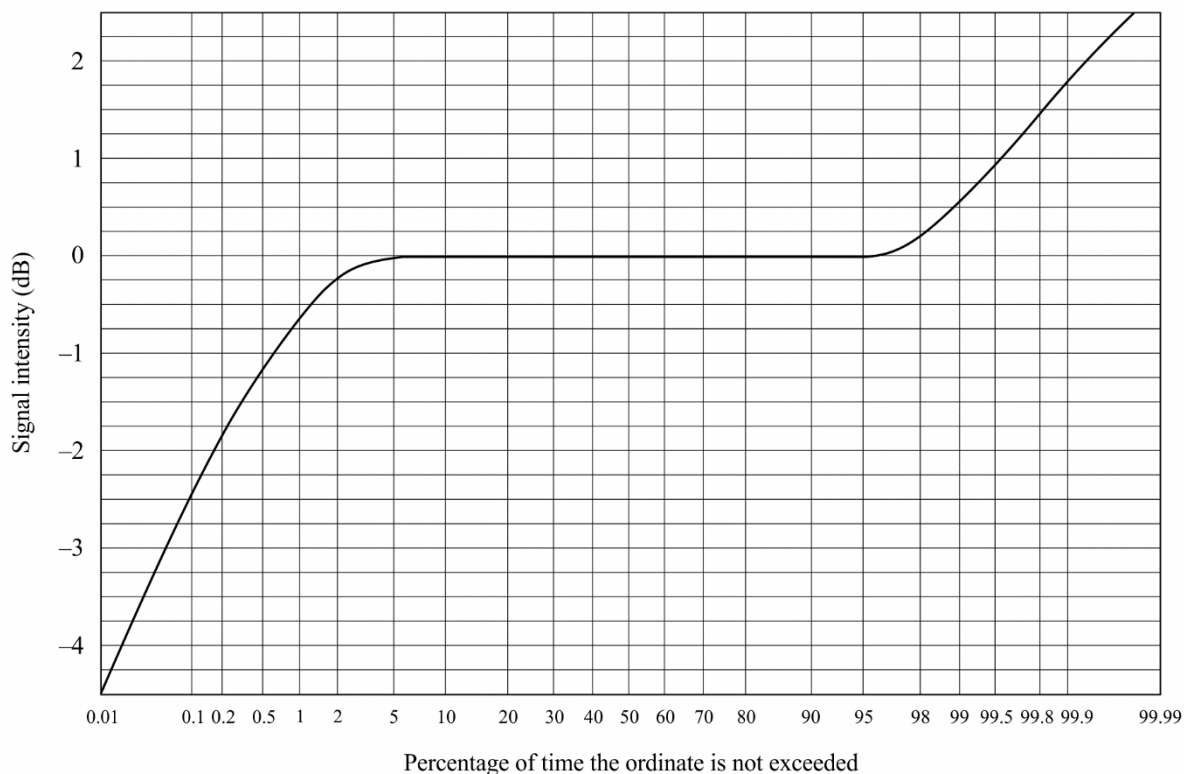
P.0531-15

6   Absorption

When direct information is not available, ionospheric absorption loss can be estimated from available models according to the $(\sec i)/f^2$ relationship for frequencies above 30 MHz, where i is the zenith angle of the propagation path in the ionosphere. For equatorial and mid-latitude regions, radiowaves of frequencies above 70 MHz will assure penetration of the ionosphere without significant absorption.

Measurements at middle latitudes indicate that, for a one-way traverse of the ionosphere at vertical incidence, the absorption at 30 MHz under normal conditions is typically 0.2 to 0.5 dB. During a solar flare, the absorption will increase but will be less than 5 dB. Enhanced absorption can occur at high latitudes due to polar cap and auroral events; these two phenomena occur at random intervals, last for different periods of time, and their effects are functions of the locations of the terminals and the elevation angle of the path. Therefore for the most effective system design these phenomena should be treated statistically bearing in mind that the durations for auroral absorption are of the order of hours and for polar cap absorption are of the order of days.

6.1   Auroral absorption

Auroral absorption results from increases of electron concentration in the D and E regions produced by incident energetic electrons. The absorption is observed over a range of 10° to 20° latitude centred close to the latitude of maximum occurrence of visual aurorae. It occurs as a series of discrete absorption enhancements each of relatively short duration, i.e. from minutes up to a few hours, with an average duration of about 30 min, and usually showing an irregular time structure. Night enhancements tend to consist of smooth fast rises and slow decays. Typical magnitudes at 127 MHz are shown in Table 2.

TABLE 2

Auroral absorption at 127 MHz (dB)

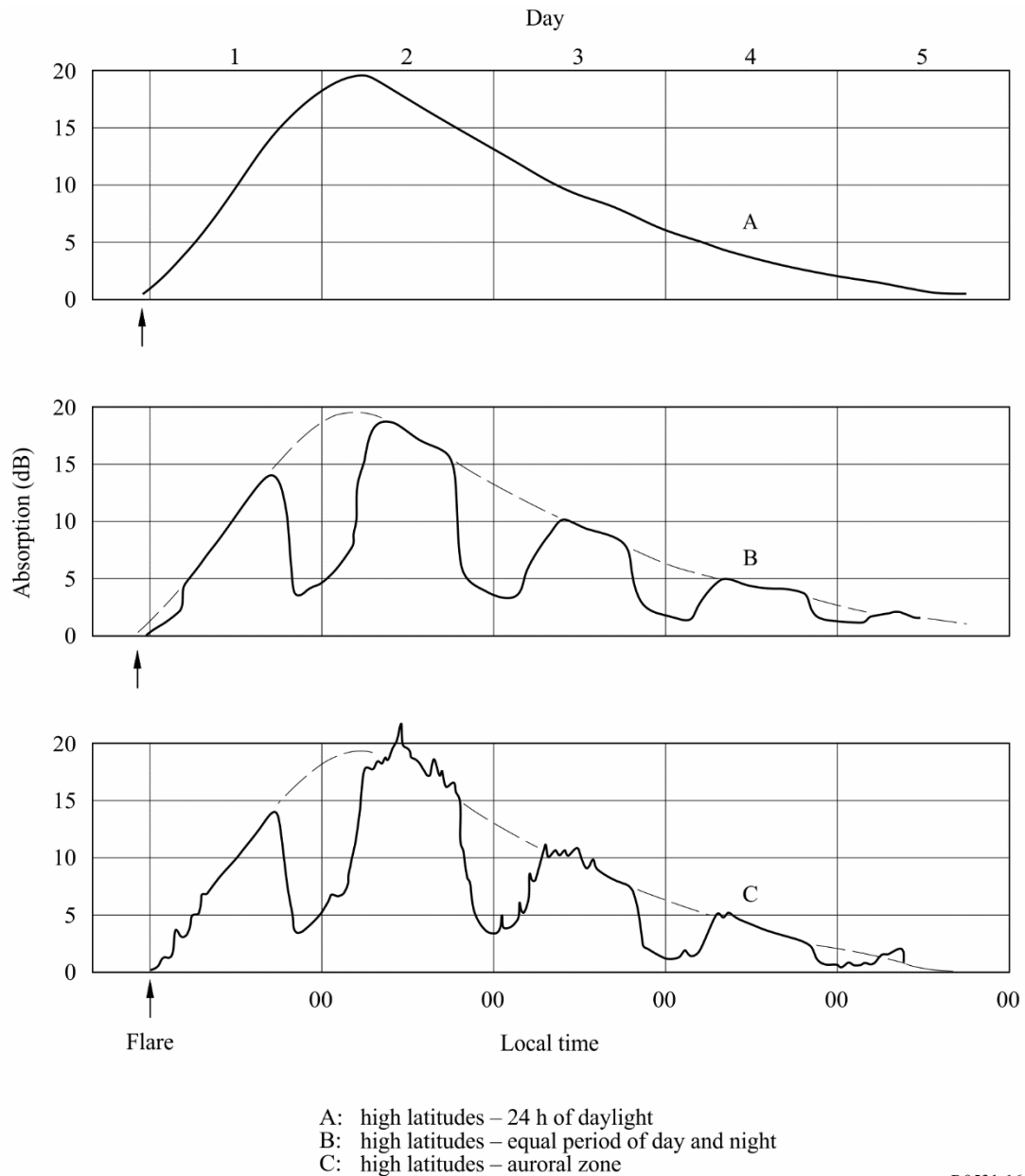| Percentage of the time	Angle of elevation	
	20°	**5°**
0.1	1.5	2.9
1	0.9	1.7
2	0.7	1.4
5	0.6	1.1
50	0.2	0.4

6.2   Polar cap absorption

Polar cap absorption which may occur at times of high solar activity, does so at geomagnetic latitudes greater than 64 degrees. The absorption is produced by ionization at heights greater than about 30 km. It usually occurs in discrete, though sometimes overlapping, events which are nearly always associated with discrete solar events. The absorption is long-lasting and is detectable over the sunlit polar caps. Polar cap absorption occurs most usually during the peak of the sunspot cycle, when there may be 10 to 12 events per year. Such an event may last up to a few days. This is in contrast to auroral absorption, which is frequently quite localized, with variations in periods of minutes.

A remarkable feature of a polar cap absorption event is the great reduction in the absorption during hours of darkness for a given rate of electron production. Figure 16 is a hypothetical model of the diurnal variation of polar cap absorption following a major solar flare based upon riometer observations at various latitudes.

FIGURE 16

**Hypothetical model showing polar cap absorption following a major solar flare
as expected to be observed on riometers at approximately 30 MHz**

A: high latitudes – 24 h of daylight
B: high latitudes – equal period of day and night
C: high latitudes – auroral zone

P.0531-16

7   Summary

Table 3 estimates maximum values for ionospheric effects at a frequency of 1 GHz. It is assumed that the total vertical electron content of the ionosphere is 10^{18} el/m^2 column. An elevation angle of about 30 degrees is also assumed. The values given are for the one-way traversal of the waves through the ionosphere.

TABLE 3

**Estimated maximum ionospheric effects at 1 GHz for elevation angles
of about 30 degrees one-way traversal**

Effect	Magnitude	Frequency dependence
Faraday rotation	108°	$1/f^2$
Propagation delay	0.25 μs	$1/f^2$
Refraction	< 0.17 mrad	$1/f^2$
Variation in the direction of arrival	0.2 min of arc	$1/f^2$
Absorption (polar cap absorption)	0.04 dB	$\sim 1/f^2$
Absorption (auroral + polar cap absorption)	0.05 dB	$\sim 1/f^2$
Absorption (mid-latitude)	< 0.01 dB	$1/f^2$
Dispersion	0-4 ns/MHz	$1/f^3$
Scintillation	See § 4	See § 4